Submitted to

32nd International Conference on High Energy Physics, ICHEP04, August 16, 2004, Beijing
Abstract: **6-0182**
Parallel Session **6**

www-h1.desy.de/h1/www/publications/conf/conf_list.html

Deeply Virtual Compton Scattering at HERA

H1 Collaboration

Abstract

The cross section for the Deeply Virtual Compton Scattering (DVCS) process $\gamma^* p \to \gamma p$ has been measured with the H1 detector at HERA in an extended kinematic domain. Using an integrated luminosity of 26 pb^{-1}, the cross section is determined as a function of the photon virtuality Q^2 and of the photon-proton centre-of-mass energy W in the kinematic region $4 < Q^2 < 80\,\mathrm{GeV}^2$ and $30 < W < 140\,\mathrm{GeV}$. The measurement is compared with next-to-leading order perturbative QCD calculations and Colour Dipole model predictions.

1 Introduction

Deeply Virtual Compton Scattering (DVCS), sketched in figure 1a, consists of the hard diffractive scattering of a virtual photon off a proton. It contributes to the reaction $e^+p \to e^+\gamma p$ which also receives contributions from the purely electromagnetic Bethe-Heitler process (figures 1b and c) and the interference between the two processes. Previous DVCS measurements at HERA can be found in references [1–3].

The interest in the DVCS process results from the particular insight it gives into the applicability of perturbative Quantum Chromo-Dynamics (QCD) to the field of diffractive interactions. In the presence of a hard scale, the DVCS scattering amplitude factorises [6–8] into a hard scattering part calculable in perturbative QCD and parton distributions which contain the non-perturbative effects due to the structure of the proton structure. The DVCS process is similar to diffractive vector meson electroproduction, but with a real photon replacing the final state vector meson. This allows the theoretical complications and uncertainties associated with the unknown vector meson wave function to be avoided. However, even at photon virtualities Q^2 above a few GeV^2, non-perturbative effects influence the predictions and have to be modelled. The wide kinematic range in the photon virtuality, Q^2, accessible at HERA, provides a powerful probe for the interplay between the perturbative and non-perturbative regimes in QCD. Furthermore, the DVCS process gives access to the Generalised Parton Distributions (GPDs) [6, 9, 10], which are generalisations of the familiar parton distributions and incorporate information on correlations between the momenta of partons in the proton.

This paper presents a new measurement of the DVCS process, in which the cross section is extracted as a function of Q^2 and of the photon-proton centre-of-mass energy W. The measurements extend to larger Q^2 and W values than has been previously possible. The data used were taken at HERA in the year 2000 in which 920 GeV protons collided with 27.5 GeV positrons. The integrated luminosity of 26.0 pb^{-1} is 3.5 times larger than the that used in the previously published H1 cross section measurements [1, 4].

2 H1 detector

A detailed description of the H1 detector can be found in [5]. Here only the detector components relevant to the present analysis are described. The SpaCal calorimeter covers the backward[1] region of the H1 detector ($153^\circ < \theta < 177.5^\circ$). Its energy resolution for electromagnetic showers is $\sigma(E)/E \simeq 7.1\%/\sqrt{E/GeV} \oplus 1\%$. The liquid argon (LAr) calorimeter ($4^\circ \leq \theta \leq 154^\circ$) is situated inside a solenoidal magnet. The energy resolution of the LAr for electromagnetic showers is $\sigma(E)/E \simeq 11\%/\sqrt{E/GeV}$. The major components of the central tracking detector are two 2 m long coaxial cylindrical drift chambers with wires parallel to the beam direction which form the Central Jet Chamber (CJC). The measurement of charged particle transverse momenta is performed in a magnetic field of 1.15 T, uniform over the full tracker volume. The forward components of the detector, used here to tag hadronic activity at high pseudorapidity

[1] H1 uses a right-handed coordinate system with the z axis pointing along the beam direction, the $+z$ or "forward" direction being that of the outgoing proton beam. Polar angles θ are measured with respect to the z axis. The pseudo-rapidity is defined by $\eta = -\ln\tan\theta/2$.

($5 \lesssim \eta \lesssim 7$), are the forward muon spectrometer (FMD) and the proton remnant tagger (PRT). The FMD, designed to identify and measure the momentum of muons emitted in the forward direction, contains six active layers, each made of a pair of planes of drift cells. The three layers between the main calorimeter and the toroidal magnet can be reached by secondary particles arising from the interaction of particles scattered under small angles hitting the beam collimators or the beam pipe walls. Secondary particles or the scattered proton at large $|t|$ can also be detected by the Proton Remnant Tagger (PRT), located at 24 m from the interaction point and consisting of double layers of scintillator surrounding the beam pipe.

3 Event selection

The cross section for the Bethe-Heitler (BH) process, which proceeds via Bremsstrahlung from the positron lines, is largest when the positron and the photon are both produced in the backward direction. In the DVCS case, the final state photon does not originate from the positron and therefore the ratio of the DVCS to the BH cross section is expected to increase when the photon is found in the forward direction. The analysis is thus restricted to the case where the photon is detected in the central or in the forward parts of the detector, i.e. in the LAr calorimeter. A data sample dominated by Bethe-Heitler events is used as a reference sample to monitor the detector's performance and the simulation thereof. Two event samples are selected according to:

- **DVCS candidate sample:** The photon candidate is detected in the LAr calorimeter and the positron candidate in the SpaCal calorimeter. Both DVCS and Bethe-Heitler processes are expected to contribute to this sample with similar magnitudes.
- **BH dominated sample:** The photon candidate is detected in the SpaCal calorimeter and the positron candidate in the LAr calorimeter. The contribution of DVCS to this sample is negligible.

The event selection is based on the detection of exactly two electromagnetic clusters, corresponding to the final state photon and positron. One cluster is required to be detected in the SpaCal calorimeter with energy larger than $15\,\mathrm{GeV}$ and the other in the LAr calorimeter ($25^\circ - 145^\circ$) with a transverse momentum $p_t > 2\,\mathrm{GeV}$. Events with more than one track reconstructed in the CJC are rejected. Events with one track are only kept if the track is associated with one of the clusters and hence identifies the positron candidate. In order to reject inelastic and proton dissociation events, no further cluster in the LAr calorimeter with energy above $0.5\,\mathrm{GeV}$ is allowed and an absence of activity above the noise level in forward detectors PRT and FMD is required. The influence of radiative corrections is reduced by requirements on the longitudinal momentum balance[2]. To enhance the DVCS signal with respect to the Bethe-Heitler contribution and to maintain a large detector acceptance, the kinematic domain is explicitly restricted to $Q^2 > 4\,\mathrm{GeV}^2$, $|t| < 1\,\mathrm{GeV}^2$ and $30 < W < 140\,\mathrm{GeV}$. The kinematic variables are reconstructed as described in section 5. Note that for the BH process, the Q^2 and W variables cannot be associated with the photon virtuality and the $\gamma^* p$ centre-of-mass energy.

[2]The quantity $\sum E - P_z$ is required to be above $45\,\mathrm{GeV}$, where E denotes the energy and P_z the momentum along the beam axis of the final state particles. The sum is calculated for the final state positron and photon.

4 Theoretical predictions

Calculations of the DVCS cross section have been published based on both NLO QCD calculations [12–14] and on Colour Dipole models [15, 16]. Both approaches contain "soft" (non-perturbative) and "hard" contributions.

Freund and McDermott [12, 13] have calculated the NLO QCD amplitude at leading twist. The soft contribution is based on the aligned jet model [17]. In a recent publication, Freund [14] has included the twist-3 contribution and proposes a parametrisation of the GPD based on standard (forward) parton densities and a squared four-momentum transfer to the proton (t) dependence of the form $\exp(bt)$ with $b = b_0(1 - 0.15\log(Q^2/2))$.

Colour Dipole models are based on the factorisation of the incoming photon wave function, the $q\bar{q}$-p cross section and the outgoing photon wave function. The main difference between the models is the way the $q\bar{q}$-p dipole cross section is parameterised. Donnachie and Dosch [15] associate soft pomerons with large dipole sizes and hard pomerons with small dipoles. Favart and Machado [16] apply the saturation model of Golec-Biernat et al. [18] to the DVCS process, including the possibility of DGLAP evolution [19]. These predictions only provide the scattering amplitude at $t = t_{min} \simeq -m_p^2 Q^4/W^4$. In both cases an exponential t-dependence, e^{bt}, is assumed.

5 Kinematic variables and Monte Carlo simulation

The reconstruction of the kinematic variables Q^2 and Bjorken x relies on the polar angle measurements of the final state electron, θ_e, and photon, θ_γ, (double angle method):

$$Q^2 = 4E_0^2 \frac{\sin\,\theta_\gamma\,(1+\cos\theta_e)}{\sin\,\theta_\gamma + \sin\,\theta_e - \sin\,(\theta_e + \theta_\gamma)}\,; \tag{1}$$

$$x = \frac{E_0}{E_p}\frac{\sin\,\theta_\gamma + \sin\,\theta_e + \sin\,(\theta_e + \theta_\gamma)}{\sin\,\theta_\gamma + \sin\,\theta_e - \sin\,(\theta_e + \theta_\gamma)}\,; \tag{2}$$

$$W^2 = \frac{Q^2}{x}\,(1-x)\,, \tag{3}$$

where E_0 and E_p are the electron and the proton beam energies, respectively. If no event vertex is reconstructed, the nominal ep interaction vertex position is assumed for the reconstruction of these angles. The variable t is very well approximated by the negative square of the transverse momentum of the outgoing proton. The latter is computed as the vector sum of the transverse momenta of the final state photon $\vec{p}_{t_\gamma}$ and of the scattered positron $\vec{p}_{t_e}$:

$$t \simeq -|\vec{p}_{t_\gamma} + \vec{p}_{t_e}|^2\,. \tag{4}$$

Monte Carlo simulations are used to estimate the corrections that must be applied to the data due to the effects of the acceptance and resolution of the detector. The generated events are passed through a detailed simulation of the H1 detector and are subject to the same reconstruction and analysis chain as the data. The Monte Carlo TINTIN [4] is used to model the

DVCS and BH processes and their interference. These contributions are simulated according the prediction of Frankfurt, Freund and Strikman [11], denoted FFS in the following. In order to subtract the small background contributions, DIFFVM [20] is to simulate diffractive vector meson electroproduction and GRAPE [21] to model electron pair production via photon-photon interactions.

6 BH dominated sample

In order to monitor the detector response in the energy and angular range relevant for the DVCS sample, the kinematic cuts on Q^2 and W used in that case are also applied to this sample, treating the photon candidate in the SpaCal as the scattered positron and the positron candidate in the LAr calorimeter as the photon. Background contributions from inelastic Bethe-Heitler events, diffractive ρ meson production and electron pair production are considered. In figure 2 the distributions of several basic quantities are compared with the simulation. A good description of the data by the sum of the different MC samples is achieved, showing that the detector response is well described by the simulation. Figure 2f), in which the transverse momentum of the positron measured by the LAr calorimeter is compared with that measured using the track curvature, illustrates the good calibration of the LAr calorimeter.

7 DVCS candidate sample

This sample is dominated by the DVCS contribution, although the contribution of the Bethe-Heitler process is not negligible. Significant contamination arises from the DVCS process with proton dissociation:

$$e^+ + p \rightarrow e^+ + \gamma + Y, \tag{5}$$

when the decay products of the baryonic system Y are not detected in the forward detectors. This typically occurs if the mass of the system for Y is below 1.6 GeV. The sum of the DVCS and BH contributions in which the proton does not survive intact has been estimated to be $11 \pm 6\,\%$ of the final sample. The other sources of background considered are diffractive ω and ϕ production as the ω and ϕ have decay modes to final states including photons (directly or from π^0 decays) or K^0_L mesons.

Figure 3 shows both data distributions and the sum of the predictions of the FFS calculation and the expected backgrounds. All contributions are normalised to the luminosity of the data sample, using a t slope of $b = 7$ GeV^{-2} for the FFS prediction. The pure Bethe-Heitler contribution is also shown. The kinematic distribution of the DVCS signal is different to that of the Bethe-Heitler contribution, in particular in the polar angle of the LAr cluster (figure 3e) and in the coplanarity (figure 3c), which is defined as the difference of the azimuthal angles of the two clusters and is related to the p_t-balance of the positron-photon system. For $|t| > |t_{min}|$, the coplanarity is expected to deviate slightly from 180° since the $e\gamma$ system must balance the transverse momentum of the scattered proton. The coplanarity distribution is found to be broader in the DVCS candidate sample than in the Bethe-Heitler dominated sample (figure 2c). This is

attributed to the electromagnetic nature of the BH process, which implies a steeper t distribution for this process than for the DVCS signal. The distributions of the kinematic variables Q^2, W and t are shown in figure 4 as are the same distributions for the sum of the predictions of the FFS calculation and the expected backgrounds.

8 Cross section measurement

To extract the cross section, the DVCS candidate sample is corrected for detector effects and for the initial state radiation of real photons from the positron line using the Monte Carlo simulation. The contamination resulting from inelastic BH and DVCS events with proton dissociation is subtracted statistically bin by bin. The background contributions from diffractive ω and ϕ production, estimated to be 3.5% on average and below $6\,\%$ in all bins, are also subtracted bin by bin.

In the leading twist approximation, the contribution of the interference term to the cross section is proportional to the cosine of the angle between the plane formed by the incoming and the scattered positron and the γ^*-proton plane. Since the present measurement is integrated over this angle, the overall contribution of the interference term is negligible. Therefore the Bethe-Heitler cross section can be subtracted from the total cross section in order to obtain the DVCS cross section. The DVCS $e^+p \to e^+\gamma p$ cross section is then converted to a DVCS $\gamma^* p \to \gamma p$ cross section using the equivalent photon approximation (as used in [22]):

$$\frac{d\sigma_{e^+p\to e^+p\gamma}}{dQ^2dy} = \Gamma(Q^2, y)\ \sigma_{\gamma^*p\to\gamma p}(Q^2, y)\ , \tag{6}$$

where $\Gamma(Q^2, y)$ is the virtual photon flux factor. In order to apply bin centre corrections, $\sigma_{\gamma^*p\to\gamma p}$ is parameterised as:

$$\sigma_{\gamma^*p\to\gamma p}(Q^2, y) \sim y^a\ (\frac{1}{Q^2})^n. \tag{7}$$

The values of the parameters a and n are obtained from an iterative fit procedure, yielding $a = 0.49 \pm 0.22$ and $n = 1.72 \pm 0.31$. This corresponds to the data following a dependence $\sigma(W) \sim W^\delta$, with $\delta = 0.98 \pm 0.44$.

The dominant systematic uncertainties arise from the following sources:

- uncertainty on the proton dissociation subtraction ($11 \pm 6\%$);
- uncertainty on the acceptance and bin centre corrections ($\pm 7\%$);
- energy calibration of the two clusters (SpaCal $\pm 1\%$, LAr $\pm 2\%$), yielding an error of 5% in both cases;
- θ measurement of the two clusters (positron ± 1.3mrad, photon ± 3mrad), yielding errors of 5% and 2%, respectively;
- uncertainty on the t slope used in the MC for the correction of detector effects ($b \pm 2$ GeV^{-2}), yielding an error of 4%;

- uncertainty on the noise in the forward detectors ($2.7 \pm 0.1\%$);
- uncertainty on the CJC random noise ($\pm 2\%$);
- uncertainty on the luminosity measurement ($\pm 1.5\%$).

9 Results

The $\gamma^* p$ cross section for the DVCS process is shown in figures 5, 6 and 7 as a function of Q^2 for $W = 82\,\text{GeV}$ and as a function of W for $Q^2 = 8\,\text{GeV}^2$. In figure 5, the measurement is compared to the NLO QCD prediction using two different GPD parameterisations [14]. The bands presented in the plot, corresponding to $5 < b_0 < 9\,\text{GeV}^{-2}$, represent the normalisation uncertainty associated with the predictions. The NLO QCD predictions are in good agreement with the data for both GPD parameterisations. The main difference between the results obtained using the two parameterisations is a change in the overall normalisation, emphasizing the need for a direct measurement of the t dependence. In figure 6, the measurement is compared to two different Colour Dipole model predictions, by Donnachie and Dosch [15] and by Favart and Machado [16]. For clarity's sake, no normalisation uncertainty band is shown in the figure. The predictions are presented for $b = 7\ \text{GeV}^{-2}$. All the Colour Dipole model predictions shown describe the data well in both shape and normalisation for the same b value. The value of $b = 7\,\text{GeV}^{-2}$ is chosen as it leads to a good representation of the normalisation and also to a good description of the uncorrected t distribution (see figure 4c). Figure 7 shows a comparison of the new measurement with the previous measurements of H1 [1] and ZEUS [2]. The two H1 measurements are in good agreement. The new H1 measurement is in fair agreement with the ZEUS results. In the region around $W \sim 70\,\text{GeV}$, the ZEUS points lie above those of, the discrepancy being at about the two standard deviation level.

10 Conclusion

The $\gamma^* p \to \gamma p$ cross section for the DVCS process is measured in an extended kinematic regime, $4 < Q^2 < 80\,\text{GeV}^2$, $40 < W < 140\,\text{GeV}$ and $|t| < 1\,\text{GeV}^2$, using a data sample taken with the H1 detector which corresponds to an integrated luminosity of 26 pb^{-1}. The measured cross section is in reasonable agreement with previous H1 and ZEUS measurements. The cross section has been compared with NLO QCD predictions [12] using GPD parameterisations based on MRST2001 and CTEQ6 [14] parton distribution functions, and to Colour Dipole model predictions [15, 16] which all describe the measured Q^2 and W distributions within errors, assuming a t slope parameter $b = 7\,\text{GeV}^{-2}$.

References

[1] C. Adloff *et al.* [H1 Collaboration], *Phys. Lett.* **B 517** (2001) 47, [hep-ex/0107005].

[2] ZEUS Collaboration, DESY-03-059, [hep-ex/0305028].

[3] A. Airapetian *et al.* [HERMES Collaboration], Phys. Rev. Lett. **87** (2001) 182001 [hep-ex/0106068].

[4] R. Stamen, PhD dissertation, Universität Dortmund and Univ. Libre de Bruxelles, DESY-THESIS-2001-057, available through:
http://www-h1.desy.de/publications/theses_list.html.

[5] I. Abt *et al.* [H1 Collaboration], Nucl. Instrum. Meth. A **386** (1997) 310 and 348.

[6] A. V. Radyushkin, Phys. Rev. **D 56** (1997) 5524 [hep-ph/9704207].

[7] J. C. Collins and A. Freund, Phys. Rev. **D 59** (1999) 074009 [hep-ph/9801262].

[8] X. Ji and J. Osborne, Phys. Rev. **D 58** (1998) 094018 [hep-ph/9801260].

[9] D. Müller, D. Robaschik, B. Geyer, F. M. Dittes and J. Hořejši, Fortsch. Phys. **42** (1994) 101 [hep-ph/9812448].

[10] X. Ji, Phys. Rev. Lett. **78** (1997) 610 [hep-ph/9603249].

[11] L.L. Frankfurt, A. Freund and M. Strikman, Phys. Lett. B **460** (1999) 417, [hep-ph/9806535].

[12] A. Freund and M. F. McDermott, Phys. Rev. D **65** (2002) 091901, [hep-ph/0106124].

[13] A. Freund and M. McDermott, Eur.Phys.J.C23:651-674,2002, [hep-ph/0111472].

[14] A. Freund, [hep-ph/0306012]. hep-ph/0306012.

[15] A. Donnachie and H. G. Dosch, Phys. Lett. B**502** (2001) 74-78, [hep-ph/0010227].

[16] L. Favart and M. V. Machado, accepted by Eur. Phys. J. C, [hep-ph/0302079].

[17] J. D. Bjorken and J. B. Kogut, Phys. Rev. D **8** (1973) 1341.

[18] K. Golec-Biernat and M. Wusthoff, Phys. Rev. D **60** (1999) 114023 [hep-ph/9903358].

[19] J. Bartels, K. Golec-Biernat and H. Kowalski, Acta Phys. Polon. B **33** (2002) 2853 [hep-ph/0207031].

[20] B. List, A. Mastroberardino, *DIFFVM: A Monte Carlo generator for diffractive processes in ep scattering, Proceedings of the Monte Carlo Generators for HERA physics*, DESY-PROC-1999-02, p. 396.

[21] T. Abe et al., *GRAPE-Dilepton, Proceedings of the Monte Carlo Generators for HERA physics*, DESY-PROC-1999-02, p. 566.

[22] C. Adloff *et al.* [H1 Collaboration], Eur. Phys. J. C **13** (2000) 371 [hep-ex/9902019].

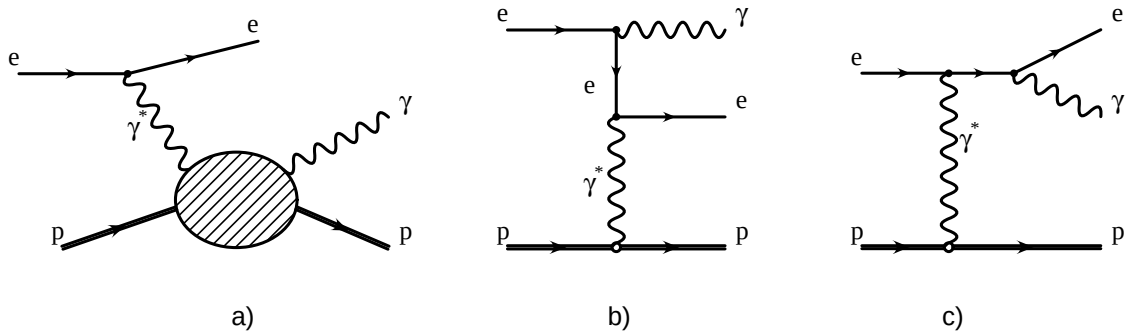

Figure 1: *Diagrams illustrating (a) the DVCS and (b and c) the Bethe-Heitler processes.*

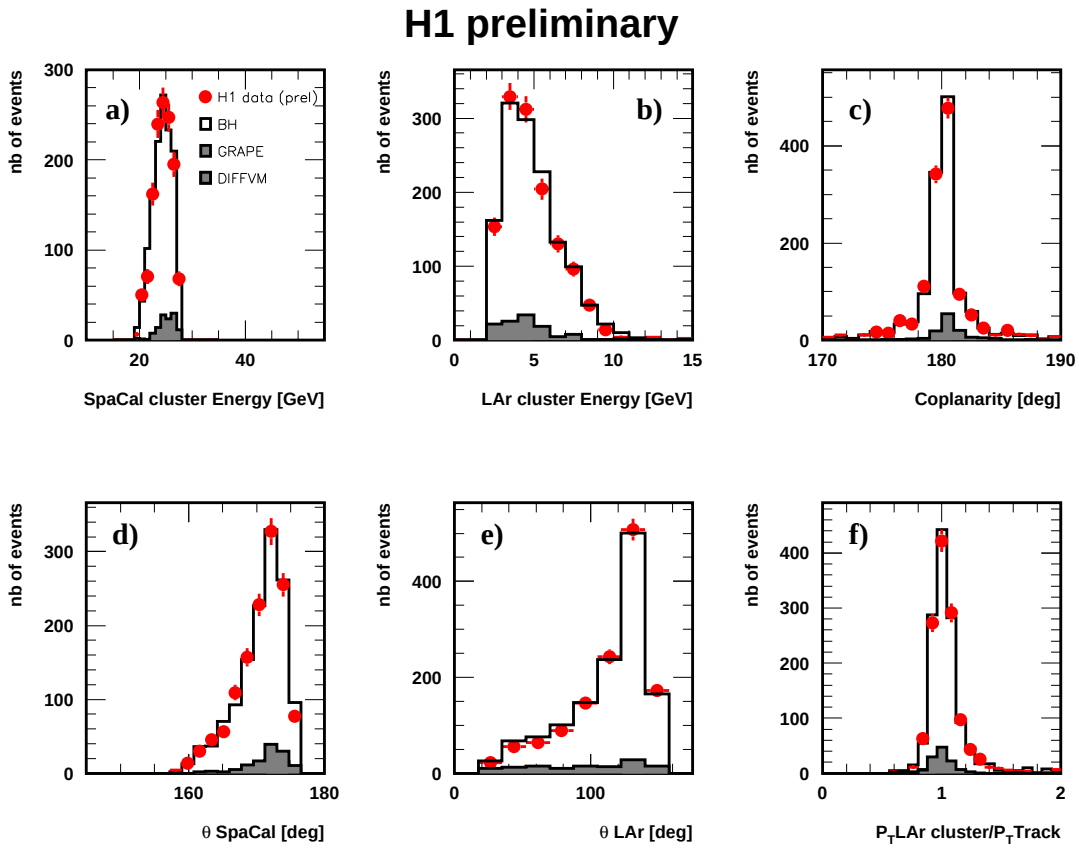

Figure 2: *Event distributions of the BH dominated sample, i.e. in which the cluster in the LAr calorimeter corresponds to the positron candidate. a) energy of the cluster in the SpaCal, b) energy of the cluster in the LAr, c) coplanarity, i.e. difference of the azimuthal angle of the positron and photon candidates, d) polar angle of the cluster in the SpaCal, e) polar angle of the cluster in the LAr, f) ratio of the transverse momentum of the positron measured with the LAr calorimeter to that determined from the track curvature. The error bars on the data points are statistical. The data are compared to the sum of the predictions for the Bethe-Heitler process, elastic dilepton production and diffractive ρ production. All predictions are normalised to the luminosity of the data.*

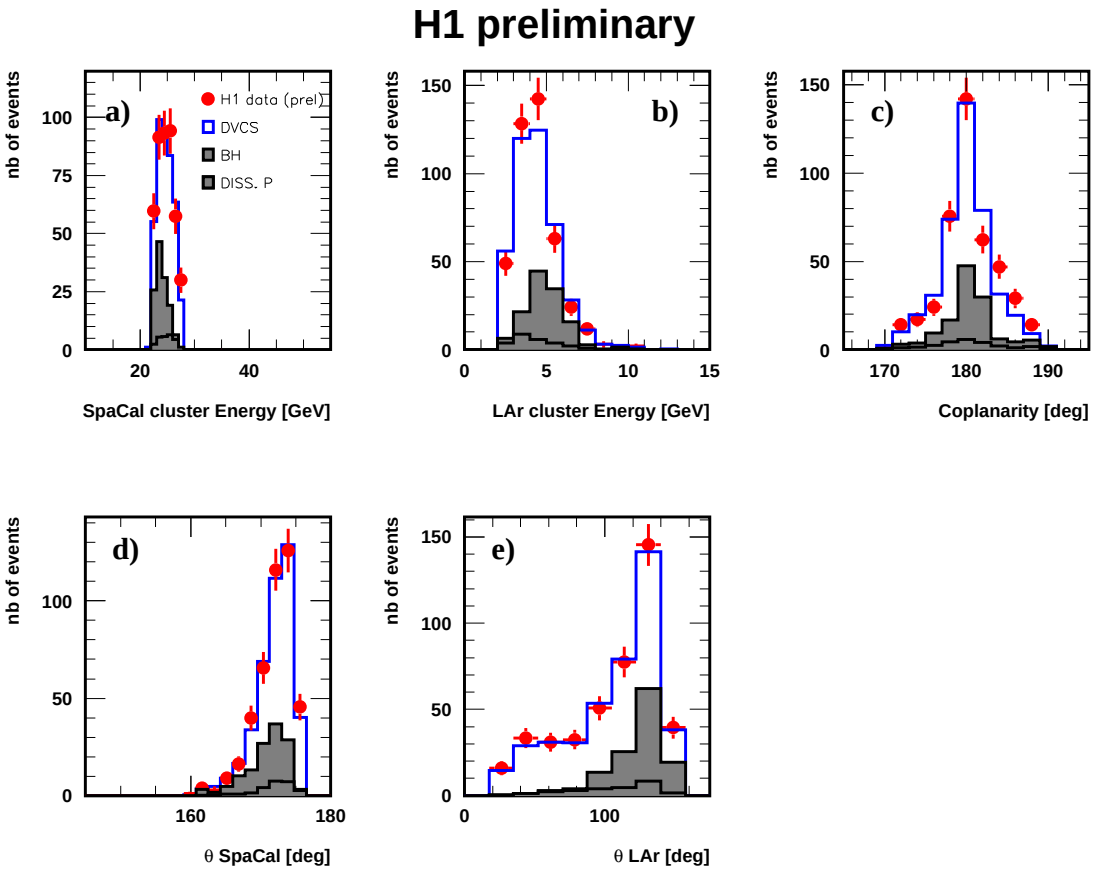

Figure 3: *Event distributions of the DVCS candidate sample, i.e. the cluster in the LAr calorimeter corresponds to the photon candidate. a) energy of the cluster in the SpaCal, b) energy of the cluster in the LAr, c) coplanarity, i.e. difference of the azimuthal angle of the positron and photon candidates, d) polar angle of the cluster in the SpaCal, e) polar angle of the cluster in the LAr. The error bars on the data points are statistical. The data are compared to the sum of the predictions for the $e^+p \to e^+\gamma p$ reaction according to FFS, using a fixed value of $b = 7$ GeV^{-2} for the DVCS calculation. All predictions are normalised to the luminosity of the data.*

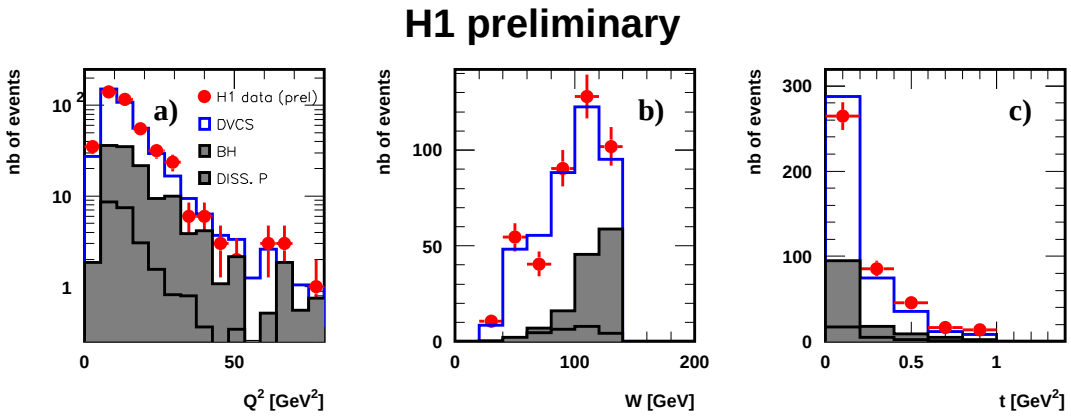

Figure 4: *Kinematic variable distributions for the DVCS candidate sample, a) Q^2, b) W c) t. The error bars on the data points are statistical. The data are compared to the sum of the predictions for the $e^+p \to e^+\gamma p$ reaction according to FFS, using a fixed value of $b = 7$ GeV^{-2} for the DVCS calculation. All predictions are normalised to the luminosity of the data.*

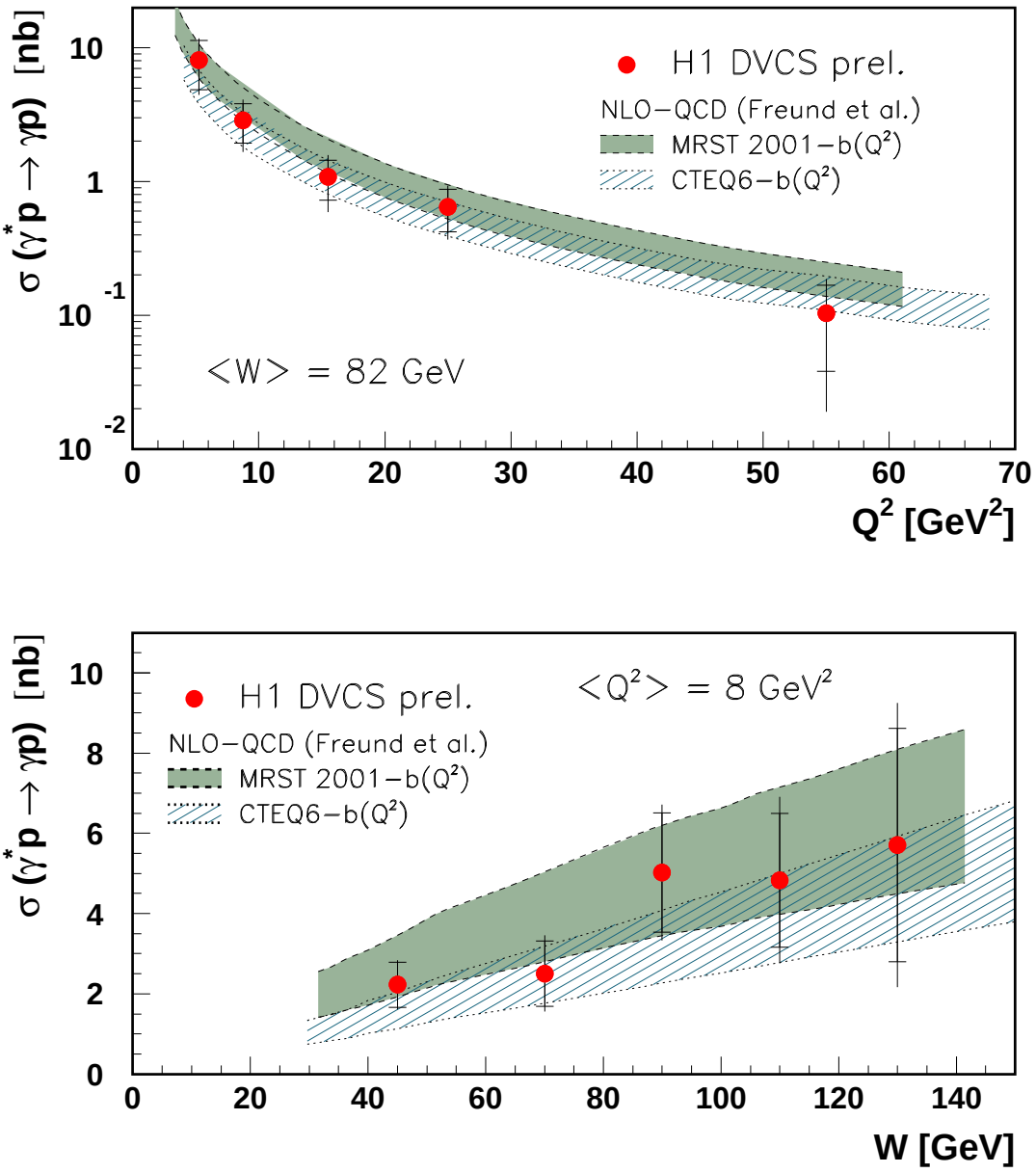

Figure 5: *The $\gamma^* p \to \gamma p$ cross section as a function of Q^2 (upper plot) for $< W >= 82$ GeV and as a function of W (lower plot) for $< Q^2 >= 8$ GeV^2. The inner error bars are statistical and the full error bars include the systematic errors added in quadrature. The measurement is compared with NLO QCD predictions [13] using two different GPD parameterisations based on MRST2001 and CTEQ6 [14] and a t dependence parameterised as e^{bt}, with $b = b_0(1 - 0.15\log(Q^2/2))$ GeV^{-2}. The bands correspond to b_0 values between 5 and 9 GeV^{-2}.*

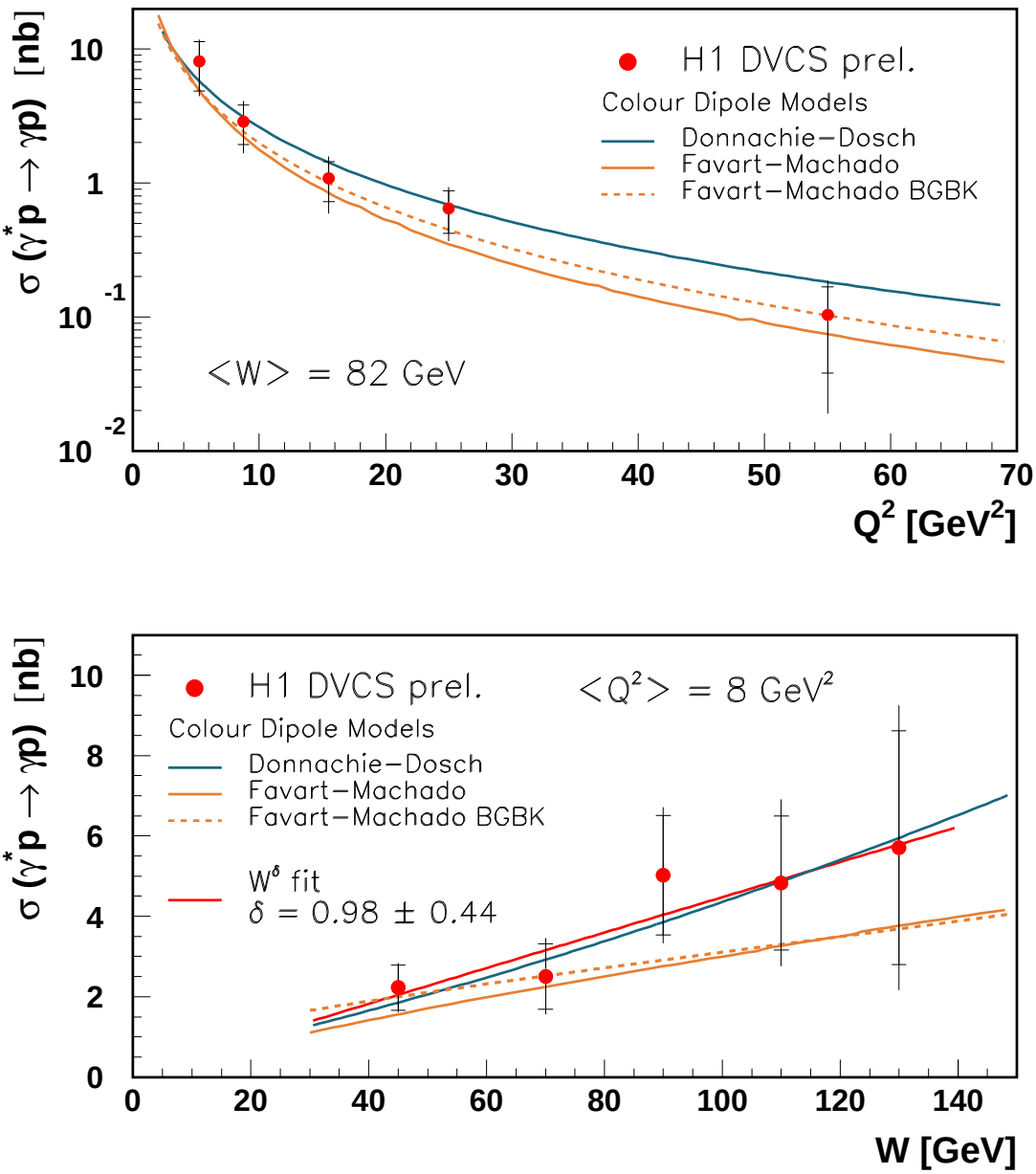

Figure 6: *The $\gamma^* p \to \gamma p$ cross section as a function of Q^2 (upper plot) for $< W >= 82$ GeV and as a function of W (lower plot) for $< Q^2 >= 8$ GeV^2. The inner error bars are statistical and the full error bars include the systematic errors added in quadrature. In addition the result of a fit of the form $\sigma(W) \sim W^{\delta}$ is shown in the lower plot. The measurement is compared with the Colour Dipole models of Donnachie and Dosch [15] and Favart and Machado [16]. The latter is shown both without and with DGLAP evolution of the dipole cross section (BGBK). In all predictions, a fixed t slope of $b = 7$. GeV^{-2} is used.*

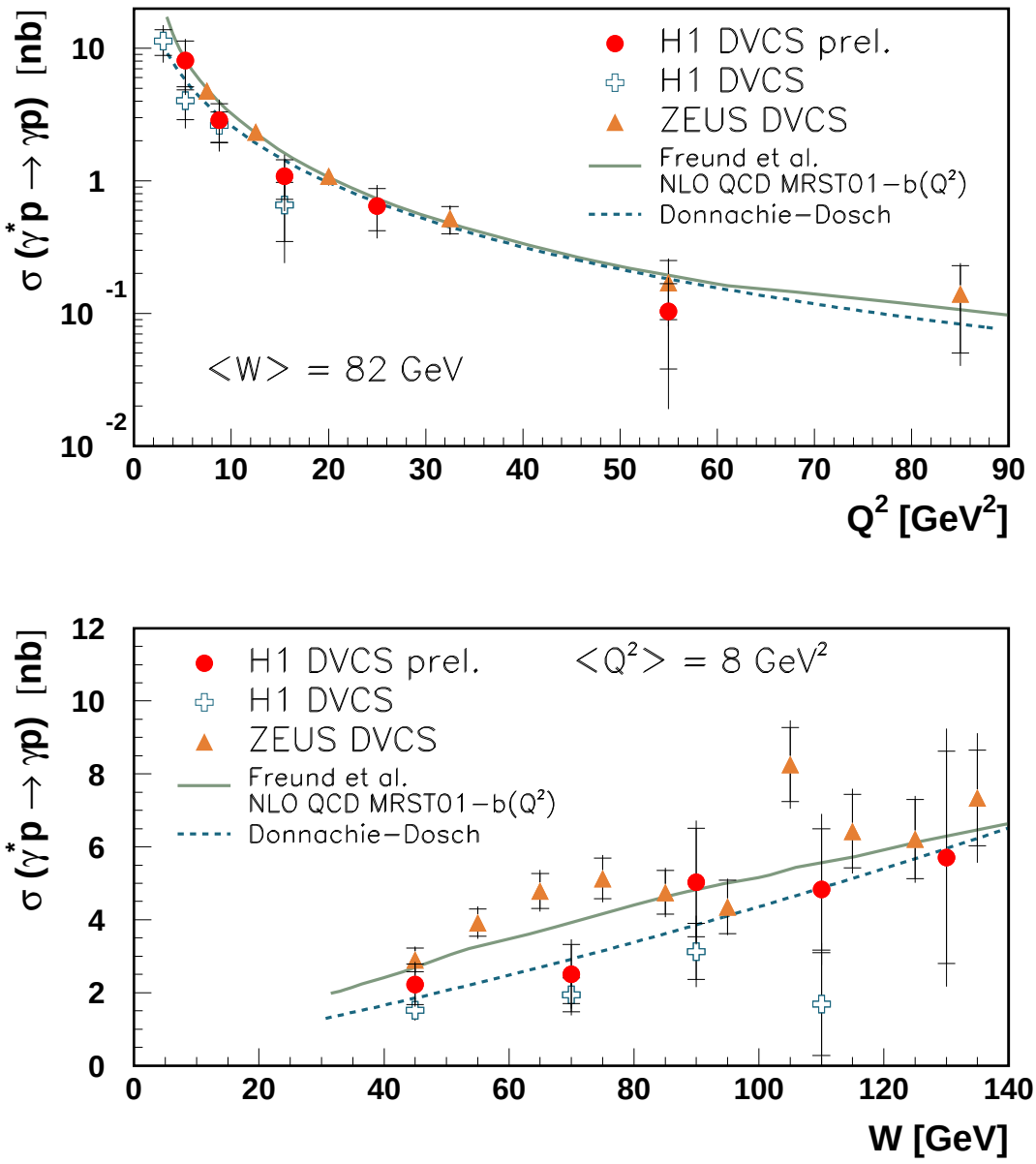

Figure 7: *The $\gamma^* p \to \gamma p$ DVCS cross section as a function of Q^2 (upper plot) for $< W >= 82$ GeV and as a function of W (lower plot) for $< Q^2 >= 8$ GeV^2. The inner error bars are statistical and the full error bars include the systematic errors added in quadrature. Previous H1 data [1] and data from the ZEUS Collaboration [2] are also shown. The measurement is compared with a NLO QCD prediction [13] using a GPD parameterisation based on MRST2001 [14] for $b_0 = 7$. GeV^{-2} and with the Donnachie and Dosch [15] Colour Dipole model prediction using $b = 7$ GeV^{-2}.*